Decadal variation of temperature inversions along Line P

Hiromichi Ueno[1]

1 Faculty of Fisheries Science, Hokkaido University, c/o Graduate School of Environmental Science, Hokkaido University, N10 W5 Kita-ku, Sapporo, Hokkaido, 060-0810 Japan.

Author for correspondence: Hiromichi Ueno, Faculty of Fisheries Science, Hokkaido University, c/o Graduate School of Environmental Science, Hokkaido University, N10 W5 Kita-ku, Sapporo, Hokkaido, 060-0810 Japan. Email: ueno@fish.hokudai.ac.jp

Abstract

Hydrographic data measured for 50 years along Line P between the North American west coast and mid Gulf of Alaska as well as data from profiling float observations were analyzed to study the formation and variation of temperature inversions in the eastern subarctic North Pacific. Remarkable decadal to inter-decadal variation was observed in the magnitude of temperature inversions. This variation was mostly attributed to the variation of southward Ekman transport, eastward geostrophic transport and surface cooling.

Keywords: Temperature inversion; Line P; Gulf of Alaska

1. Introduction

Temperature inversions (T-inversions) between subsurface temperature minima (T-min) and maxima (T-max) (see Figure 1a), are widely distributed over the subarctic North Pacific (SNP) (e.g., *Dodimead et al*., 1963; *Uda*, 1963; *Roden*, 1964; *Favorite et al.*, 1976; *Ueno and Yasuda*, 2000; 2005). Because of the presence of a strong, permanent halocline in this region, the winter mixed layer can be colder than the underlying, more saline layer, thus supporting the formation of T-inversions. In early spring, the upper portion of the winter mixed layer begins to warm, leaving the bottom portion as a T-min. In the next winter, subsurface T-min water is again entrained by the mixed layer, and therefore can influence the sea surface temperature (SST) in the following winter (*Wirts and Johnson*, 2005). Meanwhile, it has been suggested that the T-max at the base of the T-inversion is maintained by warm and saline intermediate-water

transport from the area east of Japan to the northern Gulf of Alaska (*Ueno and Yasuda*, 2000; 2002; 2003). The T-max can also influence (increase) the SST in the SNP through entrainment into the mixed layer and upwelling (*de Boyer Montégut et al*., 2007). Given the interaction between the T-inversions and the sea surface in the SNP, understanding the mechanisms involved in their formation and variation will contribute to our knowledge of heat exchange between both the surface and subsurface, and the surface and the atmosphere in the region.

In the eastern SNP (Figure 1b), the target area of the present study, T-inversions have been found to be relatively strong in the northern and southern regions (Regions A and B in Figure 1b, respectively). Using Argo profiling float data for 2001–2005 and XBT data between Alaska and Hawaii for 1993–2005, *Ueno et al*. (2007) studied seasonal and interannual variability of T-inversions in the eastern SNP, and indicated that formation and variation of T-inversions differed between the northern and southern regions as follows. In the northern region (north of 52ºN, Region A in Figure 1b), the winter mixed layer became colder than the subsurface layer and formed T-inversions nearly every winter, causing a seasonal cycle in both T-min and the magnitude of the T-inversion (ΔT: temperature difference between T-min and T-max). Therefore, interannual variation of ΔT was closely related to that of winter SST. In the southern region (42º–48ºN, Region B in Figure 1b), T-inversions were formed by cold subsurface advection from the west except in 1998 and 1999 when strong T-inversions were formed by cold winter mixed layer due to strong surface cooling. However, formation and variation of T-inversions have not been discussed in the area around 50ºN in the eastern SNP (i.e. between the northern and southern regions), where relatively large T-inversions (ΔT > 0.3ºC) occasionally occurred, and, moreover, throughout the SNP decadal variation of T-inversions has not been discussed.

Extending the analysis in *Ueno et al*. (2007), here we examine the decadal variability of T-inversions in the area around 50ºN in the eastern SNP using temperature and salinity profiles measured for more than 50 years along Line P between the North American west coast and mid Gulf of Alaska (e.g. *Freeland*, 2007). Regular sampling along this line of stations from the Canadian west coast to 145ºW is managed by Fisheries and Oceans Canada. Using the Line P data, *Crawford et al*. (2007) studied long-term variation of temperature and salinity and found that many of the temperature and salinity changes could be understood by considering changes in wind patterns and speed. Our analysis, which concentrates on vertical temperature structure, indicates that long-term variation in T-inversions is mainly attributable to variation in zonal

wind stress, eastward geostrophic advection and surface cooling.

2. Data and Methods

We used temperature and salinity profiles along Line P archived by Fisheries and Oceans Canada (http://www.pac.dfo-mpo.gc.ca/science/oceans/data-donnees/line-p/index-eng.htm). Temperature data observed by reversing thermometers and bottle-sampled salinity data (hereafter reversing-thermometer data) were used from 1956 to 1968 (actually, data before 1960 were not used due to low data coverage in space or time) and data observed by Conductivity-Temperature-Depth (CTD) profiler were used from 1968 to 2010. The reversing thermometer observes subsurface temperature by a mechanism such that, when the bulb reservoir is inverted, the mercury in the thermometer stem separates from the bulb reservoir and captures the temperature at the time of reversing (*Emery and Thomson*, 1998). Only offshore data between 130ºW and 145ºW (Station 11–26, Figure 1b) were analyzed to avoid the variability on the continental margin, which has been reported to differ from offshore variability (e.g. *Crawford et al*., 2007). In addition to Line-P data, we used temperature and salinity profiles recorded by Argo floats (*Freeland et al.*, 2010) along the offshore part of Line P (48.5º–50.5ºN and 130º–145ºW) for 2001–2010. Argo data were downloaded from the website of the Argo Global Data Assembly Center (http://www.argo.ucsd.edu, http://argo.jcommops.org) and quality-controlled as outlined in *Oka et al*. (2007).

For each profile, we determined the potential temperature minimum (T-min) and maximum (T-max) at the top and bottom of the T-inversion, as well as the potential temperature difference between T-min and T-max (ΔT), following *Ueno and Yasuda* (2005; 2007). T-inversions with ΔT smaller than 0.01ºC were omitted. T-inversions were calculated at stations with observations at more than 20 levels between 10 dbar and 500 dbar for Line-P-CTD and Argo profiles. For reversing-thermometer data few profiles cleared the condition above; therefore T-inversions were calculated at stations with observations at more than 10 levels between 10 dbar and 500 dbar. It was reported that this relatively loose criterion of 10 levels did not affect results on climatological T-inversions (*Ueno and Yasuda*, 2005). Data at depths shallower than 10 dbar were not used. A 10-dbar running mean was applied to each profile to preclude detection of temperature inversions with small vertical scale, which were likely detected in the profiles recently observed by high-resolution CTD profiler.

Line P observation cruises were conducted very frequently during 1970s, five to ten times a year. However, more than half of the analysis period of 1960–2010, cruises were conducted less than or equal to 4 times per year. In addition, in some cruises, observations were conducted just part of the offshore Line P. Therefore we evaluated seasonal-averaged (winter: January–March, spring: April–June, summer: July–September and fall: October–December) ΔT and properties at T-max and T-min to discuss their decadal variation. In the actual seasonal-averaging procedure, we divided the study area into 5 blocks before evaluating seasonal-averaged ΔT and T-min and T-max properties in the study area of 130º–145ºW to avoid spatial bias of observation. First, we evaluated seasonal-averaged ΔT and properties at each block (130º–133ºW, 133º–136ºW, 136º–139ºW, 139º–142ºW and 142º–145ºW: e.g. 2nd to 6th columns in Table 1) when at least one observation was conducted at each block and season. Second, we evaluated the seasonal-averaged ΔT and properties over the study area of 130º–145ºW (e.g. 7th column in Table 1) as the averages of block-averaged values in the same season. Seasonal-averaged values were calculated only when the number of block with observations was more than two, that is, when more than half of the study area was covered. During 2001–2010, when Argo floats also observed the Line P area, both Line P and Argo data were together used. The climatological seasonal-averaged ΔT and block-averaged ΔT, evaluated using ΔT averaged at each block in each season, were 0.19ºC in winter, 0.20ºC in spring, 0.21ºC in summer and 0.20ºC in fall, and 0.20ºC at 142º–145ºW, 0.24ºC at 139º–142ºW, 0.23ºC at 136º–139ºW, 0.20ºC at 133º–136ºW, 0.15ºC at 130º–133ºW, respectively, indicating that the seasonal variation was smaller than the spatial variation.

We also used NCEP/NCAR reanalysis monthly net surface heat flux (sum of long-wave, short-wave, latent and sensible heat fluxes) and wind-stress data area-averaged over the offshore part of Line P (48.5º–50.5ºN and 130º–145ºW) from 1956 to 2010 (*Kalnay et al.*, 1996). The NCEP/NCAR reanalysis daily wind-stress data were also used to evaluate area-averaged Ekman upwelling velocity and wind-stress strength $(\tau_x^2 + \tau_x^2)^{1/2}$, where τ_x and τ_y are eastward and northward components of wind stress. Delayed-time maps of absolute dynamic topography (ADT) of a merged altimeter satellite product distributed at 7-day intervals by AVISO (http://www.aviso.oceanobs.com; Collecte Localisation Satellites, 2011) were used. The ADT spatial resolution is 1/4º×1/4º, and we used the data from October 14, 1992 to December 29, 2010. From the ADT data we evaluated the averaged ADT difference between the areas of 50º–52ºN, 130º–150ºW and 47º–49ºN, 130º–150ºW, which corresponds to the eastward geostrophic surface velocity in the offshore part of Line P (5º extended to the west

from the western edge of Line P to include eastward flow entering to the Line P area).

Linear lag-correlation analysis was conducted between ΔT and forcing terms (wind-stress, Ekman upwelling, surface heat flux, etc.) to evaluate relative importance of each forcing term for the formation of T-inversion. Since seasonal-averaged ΔT had data-deficits in some years, we evaluated spring–summer (April–September) averaged ΔT by a method similar to seasonal-averaged ΔT evaluation described in the previous paragraph (period was just elongated from 3 months to 6 months). As the result, one ΔT value was obtained for one year, and correlation coefficients were calculated with lag-0, half-year-lag and 1-year-lag forcing terms.

3. Results

Figure 2a shows time-series of ΔT along the offshore part of Line P. Large ΔT (larger than 0.34ºC = average + 1 standard deviation) was observed during 1962, 1969–1975, 1989, 1999–2002 and 2007–2010 (yellow-shaded periods in Figure 2); ΔT changed in mostly decadal time-scale. It is important to note that the ΔT before 1968 was possibly underestimated due to low vertical resolution of temperature profiles based on reversing-thermometer observations. While we could not find clear relations between variations of ΔT and temperatures at T-max and T-min (Figures 2a and 2b), variations of depths and densities at T-max and T-min (Figure 2c and 2d) corresponded well to the ΔT variation. T-max and T-min were located at relatively shallow depths (less dense layers), mainly at 150–200m and 100–150m depths (~26.5 and ~26.0 kg m^{-3}), respectively, during the periods of large ΔT, but at greater depths (denser layers) during periods of small ΔT. The correlation coefficients, evaluated from spring-summer averaged data, between ΔT and T-max depth, T-min depth, T-max density and T-min density were -0.58, -0.62, -0.28 and -0.65, respectively, significant at the 95% confidence level. The winter mixed layer depth along the offshore part of Line P was reported to be around 100 m (e.g. *Suga et al*., 2004; *Freeland and Cummins*, 2005), suggesting that T-min was formed through winter mixed layer process during the periods of large ΔT.

We next discuss the mechanisms of decadal variation of T-inversion by comparing ΔT variability with zonal wind stress, net surface heat flux and ADT. We chose these three physical quantities based on previous studies. *Crawford et al*. (2007) indicated that cooling of surface (10–50 m) and subsurface (100–150 m) along the offshore part of Line P corresponded to the

relatively strong eastward wind, since eastward wind induced southward Ekman transport and thus provided Line P area with cold water from north of Line P. *Ueno et al*. (2007) indicated that winter surface cooling and cold subsurface-water transport from the west formed T-inversions in the area just southwest of Line P (Region B in Figure 1b). As an indicator of subsurface geostrophic zonal velocity, we used meridional ADT difference across Line P, assuming that geostrophic-flow change tendency was similar between the surface and subsurface around Line P area.

Figure 2e shows time-series of zonal wind stress, whose positive value indicates southward Ekman transport (Arrow "Ek" in Figure 1). The winter mixed layer north of Line P is cold compared with that along the Line P (e.g. *Suga et al*., 2004), suggesting that strong eastward wind stress enhances cold surface water advection from the north and therefore forms strong T-inversions. Zonal wind stress was relatively strong during 1960–1976 and 1998-2010, and relatively weak during 1977–1997, which mostly corresponded to the ΔT variation that large ΔT more frequently occurred during 1960–1976 and 1999–2010. The half-year-lag correlation coefficient between ΔT and zonal wind stress was 0.40, which was significant at the 99% confidence level. This result suggests that stronger zonal winds in previous fall-winter increase southward Ekman transport, which might transport colder surface water to the Line P area and strengthen T-inversions along Line P.

As indicated in the previous paragraphs, the period of large ΔT corresponded to the period of shallow T-min and strong zonal wind stress (Figure 2a, c and e), which seemingly contradicted our speculation that strong wind induced deeper winter mixed layer thus deeper T-min. This contradiction might be possibly explained as follows. During the period of strong zonal wind stress, strong southward Ekman transport as well as wind stirring forms cold T-min at the bottom of the winter mixed layer, that is, at the depth of 100–150m. During the period of weak zonal wind stress, on the other hand, cold T-min is not formed at the bottom of the winter mixed layer, and therefore mean T-min depth defined in this study tends to be deep due to the detection of small T-inversions occurring at the deeper layer. In addition, we examined the time variation of Ekman upwelling and wins-stress strength (Figures 2f and 2g), which also might be expected to influence the depth of T-inversion. However, no clear relationship was observed between Ekman upwelling and T-inversion depth nor between Ekman upwelling and ΔT, and strong wind stress did not correspond to deep T-min and T-max (correlations were insignificant at the 90% confidence level).

The relation between ΔT and the other possible formation mechanisms of T-inversion (surface cooling (Figure 2h) and eastward geostrophic advection (Arrow "Geo" in Figure 1 and Figure 2i) was next investigated. Surface cooling was relatively strong during the periods of 1965–1975 and 1998–1999, which mostly corresponded to periods of large ΔT. Among them, surface cooling was particularly strong in 1968–1969 and 1998–1999, when the 3rd largest and the largest ΔT were observed, respectively. Correlation coefficients between the ΔT and surface cooling were 0.33 for half-year lag, which were significant at the 95% confidence level. These results suggests that surface cooling in previous fall-winter contributed to the formation of T-inversions although the correlations were weak compared to those with southward Ekman transport. On the other hand, strong eastward geostrophic advection occurred during 2001–2002 and 2008–2009 (Figure 2i). Both periods corresponded to the large ΔT period, and the 0-lag correlation coefficient was 0.53, which was significant at the 99% confidence level. This suggests that strong eastward geostrophic advection induces strong T-inversions along the line P at least for the period of 1993–2010.

4. Conclusions

We investigated the formation and variation of T-inversions in the eastern SNP through analysis of hydrographic data measured for 50 years along Line P between the North American west coast and mid Gulf of Alaska as well as data from Argo profiling float observations. Remarkable decadal to inter-decadal variation was found in ΔT for the first time; ΔT was relatively large during 1962, 1969–1975, 1989, 1999–2002 and 2007–2010. This variation was possibly caused by the variation of southward Ekman transport, geostrophic transport from the west and surface cooling.

The results of the present study are consistent with previous studies. *Crawford et al*. (2007), who investigated Line P temperature and salinity from 1956 to 2005, reported that surface and subsurface water was relatively cold during the periods of 1964–1976, 1989–1991 and 1999–2004 (see their Figure 5), which were similar to the large ΔT periods of the present study. They further indicated that warming in 1977 was caused by weakening of southward Ekman transport and Ekman upwelling due to wind change associated with Pacific Decadal Oscillation (PDO) and that cooling in 1999 was caused by strengthening of southward Ekman transport due to wind change associated with Victoria mode, also described as the North Pacific Gyre

Oscillation (*Di Lorenzo et al*., 2009). In the present study, in addition, large ΔT is also attributed to cold-water advection due to strong eastward geostrophic flow at least for the period of 1993–2010. This is consistent with the previous studies indicating that anomalously cold subsurface water observed in 2002 along Line P was formed by strong eastward geostrophic flow (e.g. *Freeland et al*., 2003; *Crawford et al*., 2007).

The formation mechanism of T-inversions along offshore Line P in the present study was a combination of those for north of Line P (north of 52ºN: surface cooling) and for south of Line P (42º–48ºN: mainly eastward geostrophic advection) (*Ueno et al.*, 2007). For example, for strong T-inversions during 1999–2002, the former half corresponded to strong surface cooling and southward Ekman transport and the latter half corresponded to strong eastward geostrophic flow, suggesting that all three factors contributed to the formation of T-inversions in the offshore Line P area.

Acknowledgments

The author would like to thank W. Crawford for his helpful comments and fruitful discussions. The author also would like to thank S. Okkonen and two anonymous reviewers for their helpful comments. We used ocean data along Line P archived by Fisheries and Oceans Canada at the Institute of Ocean Sciences (http://www.pac.dfo-mpo.gc.ca/science/oceans/data-donnees/line-p/index-eng.htm). Line-P is managed and maintained by staff who work for Fisheries and Oceans Canada at the Institute of Ocean Sciences. The author thanks them for their efforts. The Argo float data used in this study were collected and made freely available by the International Argo Project and the national programs that contribute to it (http://www.argo.ucsd.edu; http://argo.jcommops.org). Argo is a pilot program of the Global Ocean Observing System. The author thanks S. Matsunaga for his support.

References

Crawford WR, Sutherland P, Hardenberg PV (2005) Cold water intrusion into the Gulf of Alaska in 2002. Atmosphere-Ocean 43(2):119–128. doi:10.3137/ao.430201

Crawford WR, Galbraith J, Bolingbroke N (2007) Line P ocean temperature and salinity 1956-2005. Prog Oceanogr 75:161-178. doi:10.1016/j.pocean.2007.08.017

de Boyer Montégut C, Mignot J, Lazar A, Cravatte S (2007) Control of salinity on the mixed layer depth in the world ocean: 1. General description. J Geophys Res 112 C06011. doi:10.1029/2006JC003953.

Di Lorenzo E, Fiechter J, Schneider N, Bracco A, Miller AJ, Franks PJS, Bograd SJ, Moore AM, Thomas AC, Crawford WR, Peña A, Hermann A (2009) Nutrient and salinity decadal variations in the central and eastern North Pacific. Geophys Res Lett 36 L14601. doi:10.1029/2009GL038261.

Dodimead AJ, Favorite F, Hirano T (1963) Salmon of the North Pacific Ocean Part II: Review of Oceanography of the Subarctic Pacific Region Bull 13. International North Pacific Commission, Vancouver, pp. 195

Emery, W. J. and R. E. Thomson (1998) Data Analysis Methods in Physical Oceanography. Elsevier, New York, 636 pp.

Favorite F, Dodimead AJ, Nasu K (1976) Oceanography of the Subarctic Pacific Region, 1960–71 Bull 33. International North Pacific Commission, Vancouver, pp. 187

Freeland HJ, Roemmich D, Garzoli S, LeTraon P, Ravichandran M, Riser S, Thierry V, Wijffels S, Belbéoch M, Gould J, Grant F, Ignazewski M, King B, Klein B, Mork K, Owens B, Pouliquen S, Sterl A, Suga T, Suk M, Sutton P, Troisi A, Vélez-Belchi P, Xu J (2010) Argo—a decade of progress. In: Hall J, Harrison DE, Stammer D (eds) Proceedings of Ocean Obs'09: sustained ocean observations and information for society, vol 2, Venice, Italy, 21–25 September 2009. ESA Publication WPP-306. doi:10.5270/OceanObs09.cwp.32

Freeland HJ, Gatien G, Huyer A, Smith RL (2003) Cold halocline in the northern California Current: An invasion of Subarctic water. Geophys Res Lett 30. doi:10.1029/2003GL016663

Freeland HJ, and Cummins PF (2005), Argo: A new tool for environmental monitoring and assessment of the world's oceans, an example from the N.E. Pacific. Prog Oceanogr 64(1):31–44. doi:10.1016/j.pocean.2004.11.002

Freeland HJ (2007) A short history of Ocean Station Papa and Line P. Prog Oceanogr 75(2):120–125. doi:10.1016/j.pocean.2007.08.005

Kalnay, E., et al. (1996), The NCEP/NCAR 40-year reanalysis project. Bull Am Meteorol Soc 77(3):437–471. doi:10.1175/1520-0477(1996)077<0437:TNYRP>2.0.CO;2

Oka E, Talley LD, Suga T (2007) Temporal variability of winter mixed layer in the mid- to high-latitude North Pacific. J Oceanogr 63(2):293–307

Roden GI (1964) Shallow temperature inversion in the Pacific Ocean. J Geophys Res 69(14):2899–2914. doi:10.1029/JZ069i014p02899

Collecte Localisation Satellites (2011), SSALTO/DUACS user handbook: (M)SLA and (M)ADT near-real time and delayed time products, version 2rev4, Rep. SALP-MU-P-EA-21065-CLS, Ramonville St-Agne, France, pp. 49

Suga T, Motoki K, Aoki Y, Macdonald AM (2004) The North Pacific climatology of winter mixed layer and mode waters. J Phys Oceanogr. 34(1):3–22. doi:10.1175/1520-0485(2004)034<0003:TNPCOW>2.0.CO;2

Uda M (1963) Oceanography of the subarctic Pacific Ocean. J Fish Res Board Can 20:119–179

Ueno H, Yasuda I (2000) Distribution and formation of the mesothermal structure (temperature inversions) in the North Pacific subarctic region. J Geophys Res 105(C7):16885–16898. doi:10.1029/2000JC900020

Ueno H, Yasuda I (2001) Warm and saline water transport to the North Pacific subarctic region: World Ocean Circulation Experiment and Subarctic Gyre Experiment data analysis. J Geophys Res 106(C10):22,131–22,141. doi:10.1029/2000JC000457

Ueno H, Yasuda I (2003) Intermediate water circulation in the North Pacific subarctic and northern subtropical regions. J Geophys Res 108(C11):3348. doi:10.1029/2002JC001372.

Ueno H, Yasuda I (2005) Temperature inversions in the subarctic North Pacific. J Phys Oceanogr 35(12):2444–2456. doi:10.1175/JPO2829.1

Ueno H, Oka E, Suga T, Onishi H (2005) Seasonal and interannual variability of temperature inversions in the subarctic North Pacific. Geophys Res Lett 32(L20603). doi:10.1029/2005GL023948.

Ueno H, Oka E, Suga T, Onishi H, Roemmich D (2007) Formation and variation of temperature inversions in the eastern subarctic North Pacific. Geophys Res Lett 34(L05603).

doi:10.1029/2006GL028715.

Wirts, A. E., and G. C. Johnson (2005), Recent interannual upper ocean variability in the deep southeast Bering Sea. J Mar Res 63(2):381–405. doi: 10.1357/002224005369372

Tables

Table 1: An example demonstrating seasonal-averaged ΔT estimation in 1976. Values in the 2nd to 6th columns indicate ΔT averaged at each block in each season (and profile number used for evaluation), evaluated only when at least one profile with ΔT > 0.01ºC was obtained at the block in the season. Values in the 7th column indicate seasonal averaged ΔT as an average of values in the 2nd to 6th columns in the same row (and number of block used for evaluation). Seasonal averaged ΔT is evaluated only when block-averaged values are obtained at least 3 blocks in the season.

1975	ΔT averaged at each block in each season (profile number)					Seasonal averaged ΔT (block number)
	142º–145ºW	139º–142ºW	136º–139ºW	133º–136ºW	130º–133ºW	130º–145ºW
Winter	0.09ºC (35)	N/A (0)	0.07ºC (1)	0.02ºC (1)	0.08ºC (3)	0.06ºC (4)
Spring	0.10ºC (33)	N/A (0)	0.15ºC (2)	0.04ºC (1)	0.17ºC (1)	0.11ºC (4)
Summer	0.23ºC (27)	N/A (0)	N/A (0)	N/A (0)	0.13ºC (1)	N/A (2)
Fall	0.58ºC (27)	0.12 (1)	0.14 (3)	0.15 (3)	0.07 (2)	0.21 (5)

Table 2: Lag correlation coefficients (and p-values) between ΔT and zonal wind stress, Ekman upwelling velocity, wind stress strength, surface heat flux, and ADT difference which corresponds to surface geostrophic velocity. Values with underline indicate their correlations were significant at the 95% confidence level. Number of data used for evaluation was 51 (1960–2010) for 2nd to 5th columns and was 18 (1994–2010) for 6th column.

Lag	Zonal wind stress	Ekman upwelling	Wind stress strength	Surface heat flux	ADT difference
0	0.24 (0.09)	0.00 (1.00)	-0.01 (0.97)	-0.11 (0.42)	0.53 (0.02)
Half year	0.40 (0.00)	-0.01 (0.93)	0.15 (0.30)	0.33 (0.02)	0.17 (0.49)
1 year	0.37 (0.03)	0.05 (0.70)	0.18 (0.21)	0.29 (0.04)	0.14 (0.57)

Figure Captions

Fig. 1 (a) Vertical potential temperature profile observed at Station 24 (49.8ºN, 142.7ºW) on 13 September 2000. The ΔT, T-max and T-min are defined in the text. (b) Distributions of ΔT (°C) averaged in each 3° × 1° box using World Ocean Database 2001 (after Ueno and Yasuda, 2005). Values were not estimated (blanked out) in areas where temperature inversions seldom occur or in the area of insufficient data (see Figure 5a caption in Ueno and Yasuda, 2005). White circles with black frame denote location of offshore part of Line P data (Station 11–26). Black rectangles denote Region A (52°–60° N, 130°–160°W) and Region B (42°–48°N, 140°–160°W) discussed in Ueno et al. (2007). Arrows “Ek” and “Geo” denote southward Ekman transport and eastward geostrophic transport, respectively.

Fig. 2 Time series of (a) ΔT (°C), (b) potential temperature (°C) at T-max (red) and T-min (blue), (c) depth (dbar) at T-max (red) and T-min (blue), (d) density (kg m^{-3}) at T-max (red) and T-min (blue), (e) eastward component of wind stress (N m^{-2}), (f) Ekman upwelling velocity (10^{-7} m s^{-1}: positive value means upwards velocity) (g) wind-stress strength (N m^{-2}) (h) net surface heat flux (W m^{-2}: positive value means that ocean is cooled) and (i) area-averaged ADT difference (cm) between the areas of 50º–52ºN, 130º–150ºW and 47º–49ºN, 130º–150ºW. Values in (e) and (h) are 11-month running-mean values, and those in (f), (g) and (i) are 1-year running-mean values. In (a), (b), (c) and (e), filled (open) circles are evaluated from Line P CTD (reversing-thermometer) data, and open squares are evaluated from CTD and Argo data.

Horizontal lines in (a), (e), (f), (g) (h) and (i) denote mean ± 1 standard deviation evaluated for 1960–2010 (a, e, f, g and h) and 1993–2010 (i). Horizontal lines in (b), (c) and (d) are mean values evaluated for 1960–2010 (red: T-max and blue: T-min).

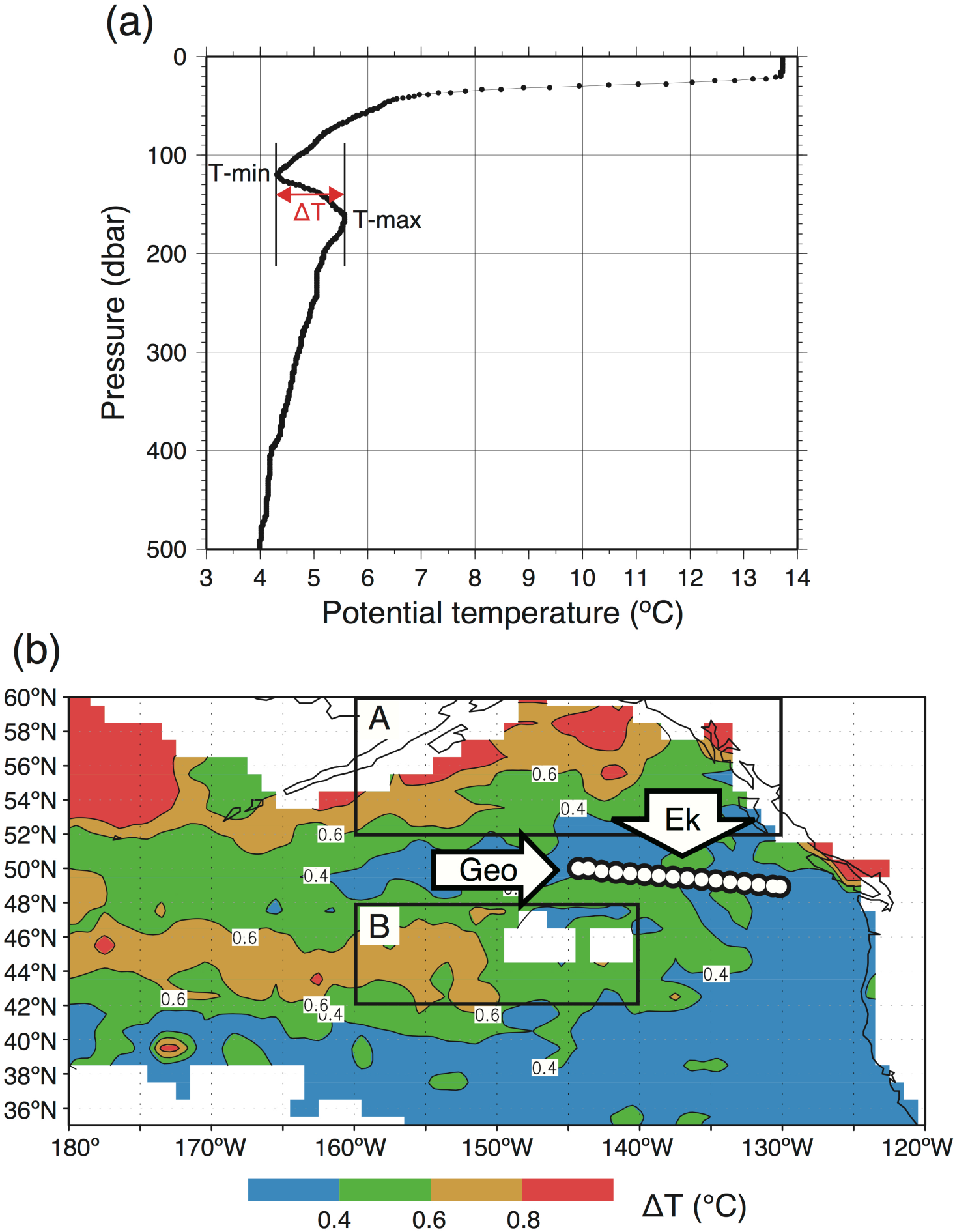
(a)
Pressure (dbar)
0
100
200
300
400
500
T-min
ΔT
T-max
3
4
5
6
7
8
9
10
11
12
13
14
Potential temperature (°C)
(b)
60°N
58°N
56°N
54°N
52°N
50°N
48°N
46°N
44°N
42°N
40°N
38°N
36°N
180°
170°W
160°W
150°W
140°W
130°W
120°W
A
B
Ek
Geo
0.6
0.4
0.4
ΔT (°C)

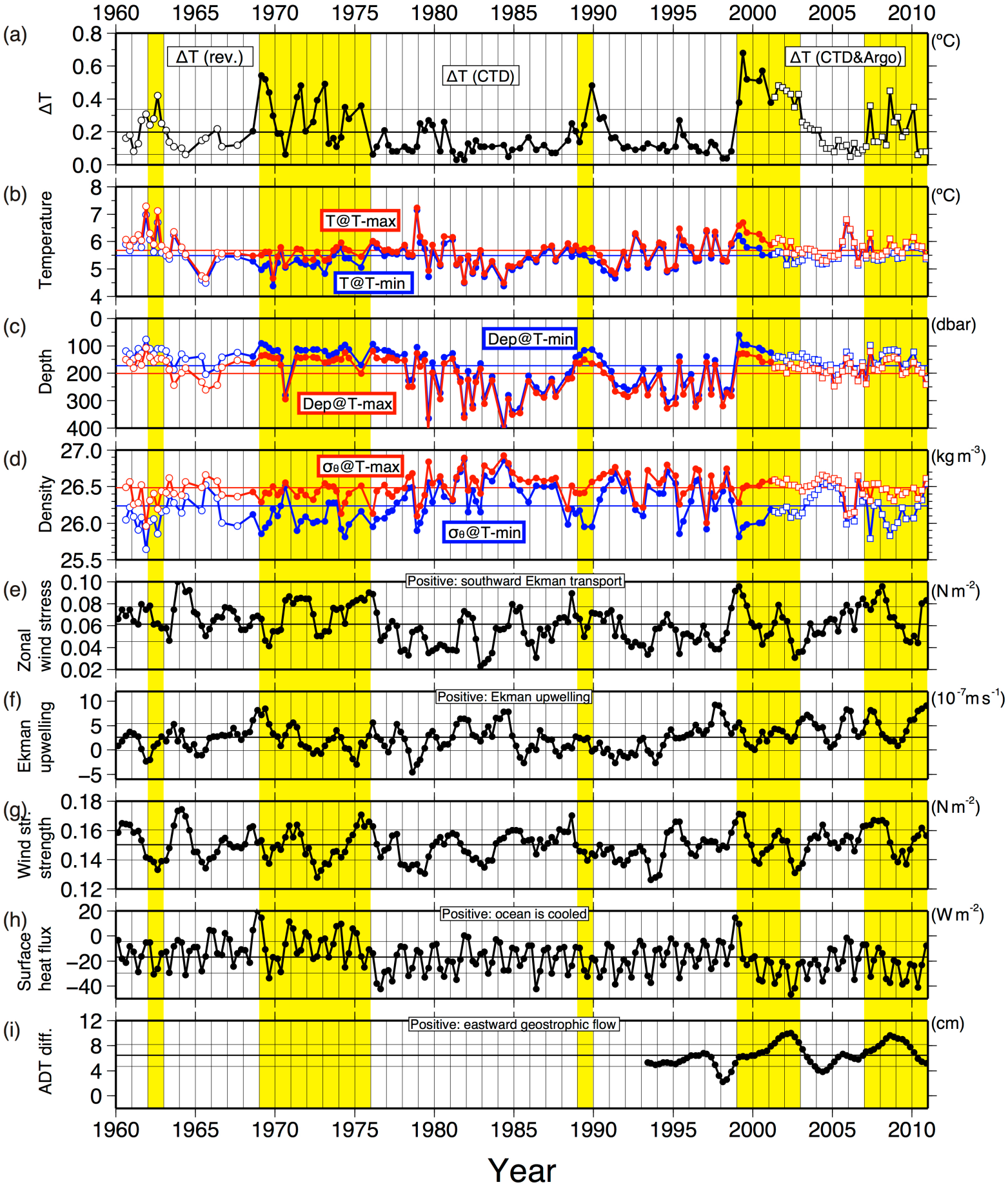
(a)
ΔT
ΔT (rev.)
ΔT (CTD)
ΔT (CTD&Argo)
(°C)
(b)
Temperature
T@T-max
T@T-min
(°C)
(c)
Depth
Dep@T-min
Dep@T-max
(dbar)
(d)
Density
σθ@T-max
σθ@T-min
(kg m-3)
(e)
Zonal wind stress
Positive: southward Ekman transport
(N m-2)
(f)
Ekman upwelling
Positive: Ekman upwelling
(10-7 m s-1)
(g)
Wind str. strength
(N m-2)
(h)
Surface heat flux
Positive: ocean is cooled
(W m-2)
(i)
ADT diff.
Positive: eastward geostrophic flow
(cm)
Year